An Investigation of the Accuracy of Manifold Methods and Splitting Schemes in the Computational Implementation of Combustion Chemistry

B. YANG* and S. B. POPE

Sibley School of Mechanical Aerospace Engineering, Cornell University, Ithaca, New York 14853-7501

This paper is concerned with the efficient computational implementation of combustion chemistry, for use in PDF methods and other applications. A new method of coupling reactions and mixing processes based on manifold points with detailed chemistry is developed. Investigations are made of three different kinds of methods: the direct numerical integration of the coupled reaction and mixing equations; the direct numerical integration of the equations obtained by using operator-splitting to split reaction and mixing; and the new method—solving the split system based on manifold points with detailed chemical kinetics. Errors between the solutions are studied. It is found that chemical reactions have a significant influence on the accuracy of operator-splitting methods. The solution of the split systems based on manifold points provides an accurate representation for the solution of the full coupled equations. This means that tabulations can be made on manifolds with no simplification made to the chemistry. © 1998 by The Combustion Institute

1. INTRODUCTION

In the last decade, great progress has been made in combustion research, especially in the computation of laminar flames [1, 2, 3, 4], and in the probability density function (PDF) method for turbulent combustion [5, 6, 7]. For one-dimensional laminar flames, by considering the transport mechanism, the detailed chemical kinetic mechanism and the interactions between these two basic processes, today it is a routine matter to calculate flame velocities, extinction, ignition, temperature and species distributions, from the governing equations. Results are in good agreement with those obtained from experiments [8, 9]. However, for turbulent combustion, because of the complexities of turbulent flow, chemical reactions, and the interaction between them, in the foreseeable future it is impossible to calculate the combustion flow field by directly integrating the basic governing equations. So averaging and modeling are necessary in turbulent combustion studies. Averaging, on one hand, sim-

plifies turbulent combustion calculations, on the other hand, it introduces the infamous closure problems, especially the closure problem with chemical reaction terms. Since in PDF calculations of turbulent combustion the averages of the chemical reaction terms can be calculated, PDF methods overcome the closure problem with the reaction terms. It has been shown that the PDF method is the most promising method to calculate turbulent combustion [6]. PDF methods have been successfully employed to calculate laboratory turbulent flames: they can predict phenomena such as super equilibrium radical levels, and local extinction [7]. Because of these advantages, PDF methods are becoming used increasingly in industrial combustor codes.

Although PDF methods have shown great promise in studies of turbulent combustion, there is still a challenge to be overcome—coupling the detailed description of the turbulent combustion flow field provided by PDF methods with detailed chemical kinetic mechanisms. The problem can be stated thus: in a PDF calculation of turbulent combustion, let $\phi(t)$ represent the composition of a particle at time t, then what is the increment in composition $\Delta\phi(t)$ due to reaction over a time step δt? In principle, this question can be answered by

---

*Corresponding author. Address: 138 Upson Hall, Box XX, Cornell University, Ithaca, New York 14853-7501. Telephone: 607-255-8270, Fax: 607-255-1222, e-mail byang@mae.cornell.edu

directly integrating the ordinary differential equations stemming from the detailed kinetic mechanism. But in practice, since a typical combustion system involves dozens of chemical species and hundreds of chemical reactions, and it is needed to do such integrations on the order of 10^9 times, the direct numerical integration of the equations would require a huge amount of supercomputer time (several hundred days) and thus make it impossible in practical use. So simplifications of detailed kinetic mechanisms have been made in the past in order to reduce the demand on computer time. In practice there is a preprocessing stage in which results from the calculations of simplified chemistry are tabulated as functions of a few variables. Then these tables are used in turbulent combustion calculations.

There are basically two different ways of doing the simplification of detailed chemistry: the reduced mechanism method [10, 11, 12] and the intrinsic low-dimensional manifold (ILDM) method [13]. For the reduced mechanism method, the simplification made to the detailed chemistry is achieved by introducing steady-state assumptions for some species, usually the intermediate species, and the partial equilibrium assumptions for particular reactions. The reduced mechanism method has been employed in laminar flame calculations and in turbulent combustion calculations [11, 14]. It has several disadvantages because of its fundamental philosophy. For the reduced mechanism method, one needs to know in advance which species are in steady-state, and which reactions are in partial equilibrium. Reduced mechanism systems are derived manually from the given detailed chemistry. For different fuel/oxidizer systems, or even for the same fuel/oxidizer system under different conditions, different reduced mechanisms should be used. Thus it requires a considerable amount of human time and labor to develop and test such systems. Assumptions of partial-equilibrium and steady-state used in the reduced mechanism method are only valid in particular reaction ranges. Also the accuracy cannot be given and controlled.

The manifold method is based on a more intrinsic study of the chemical reaction process happening in combustion [13]. As it is ob-

served, there is a wide range of time scales for chemical reactions, from 10^{-9} second to seconds. Fast reactions, or reactions with small time scales, quickly bring composition points down to attracting manifolds in the composition space. Then composition points move along on manifolds. By assuming that the movement of the composition point away from manifolds to be zero, detailed chemistry can be simplified. The manifold method overcomes the drawbacks of the reduced mechanism method. It requires no preliminary knowledge of which chemical species are in steady-state and which chemical reactions are in partial equilibrium. The only given assumption is the dimension of the manifold.

The manifold method has been successfully used in both laminar flames and turbulent combustion studies [7, 15, 16]. In these studies, a manifold with fixed dimension, for example, two dimensions, has been considered. The results from manifold calculations are tabulated in a preprocessing stage. Then the method of table-look-up is used in PDF calculations. There are still some difficulties and inconveniences with this approach to implementing manifold methods:

- in general, it is not straightforward to parametrize the manifold,
- in different regions of the composition space, manifolds of different dimension are appropriate,
- the table generation (which is not fully automated) must be performed for each set of conditions of interest (fuel, pressure, equivalence ratio, etc.),
- the whole of the manifold is (wastefully) tabulated since it is not known a priori which regions are needed.

So we have been motivated to investigate new implementations of manifold methods which can overcome these difficulties and inconveniences.

2. OUTLINE OF THE PAPER

This paper addresses several issues related to the accurate numerical implementation of combustion chemistry.

2.1. Splitting Strategies

Most numerical implementations of table-look-up chemistry correspond to the zero-order splitting strategy. That is, the evolution equations for the fluid composition with the omission of the reaction term are advanced for a small time step δt: and then the increment in composition over the time δt is added to the result. In PDF methods, the first part corresponds to mixing, and so this strategy is referred to as mix-then-react.

Important questions addressed here are: How large are the numerical errors introduced by this splitting? And, do higher-order splitting strategies offer advantages? Splitting strategies are described in Section 4, and numerical results are given in Section 6.

2.2. Variable-Dimension Manifold

In previous implementations of the intrinsic low dimensional manifold, a manifold of fixed dimension is considered. It is preferable to define the manifold instead in terms of a time scale τ^*, which is specified to be somewhat smaller than the smallest fluid-mechanical time scale in the problem (usually the mixing time scale τ_{mix}). The definition of this manifold is given in Section 5.1.

In order to implement the manifold method it is necessary to solve the "closest manifold point" problem. That is, given τ^* and a composition $\phi^{(I)}$, determine the closest point to $\phi^{(I)}$ that is on the manifold. The solution to this problem is given in Section 5.2.

2.3. Solution of the Mixing and Reaction Equation

In the overall method currently being developed, properties of the manifold are stored using "*in situ* adaptive tabulation" (ISAT). As the PDF calculation is performed, an unstructured table is generated, containing N pairs of compositions and their corresponding increments, $\{\phi^{(n)}, \Delta\phi^{(n)}, n = 1, 2, \ldots, N\}$. The table is stored in a structure that is initially empty ($N = 0$). For each particle on each time step in the PDF calculation, the increment $\Delta\phi$ is

sought based on the particle's composition ϕ. The table is searched for an entry $\phi^{(n)}$ sufficiently close to ϕ. If one exists, then $\Delta\phi^{(n)}$ is used to approximate $\Delta\phi$. If a sufficiently close table entry does not exist, then $\Delta\phi$ is computed by the direct integration of equations from detailed chemistry, and the result is added to the table. This tabulation scheme is not further described or used here. Rather we address the question: how can information about the manifold be used to determine the evolution of composition $\phi(t)$ due to mixing and reaction? The result, described in Section 5.3, is an exact solution to the equations linearized about a manifold point.

The accuracy of this solution compared to the detailed kinetics is investigated in Section 6.

2.4. Pairwise Mixing Stirred Reactor (PMSR)

A simple test case that has been used previously is the partially stirred reactor (PaSR) [17]. For a PaSR, the system can either be premixed or diffusion. The mixing model used is the interaction-by-exchange-with-the-mean (IEM) model [17]. In the statistically stationary state of a PaSR calculation, the composition $\phi(t)$ of a particle is a unique function of the particle's age (i.e., time since it entered the reactor). As a consequence, all particle compositions lie on a one-dimensional manifold since chemical reactions always pull particle composition toward the equilibrium state which is a zero-dimensional manifold; and so, in fact, the PaSR is not a strenuous test of simplified chemistry schemes.

To provide a better test case we have developed a different implementation of the PaSR, referred to as the "pairwise mixing stirred reactor" (PMSR). This is described in Section 3 and used for all of the tests reported in Section 6.

3. THE PAIRWISE MIXING STIRRED REACTOR

The PMSR is characterized by a residence time τ_{res}, a pairing time τ_{pair}, and a mixing time τ_{mix}. In numerical implementations the reactor

consists of M particles, which are arranged as $L = M/2$ pairs of particles.

At the initial time $t = 0$, the particle compositions $\phi^{(n)}(0)$ are initialized to the chemical equilibrium state.

With Δt being a time step, "reactor events" take place at the discrete times, $\Delta t, 2\Delta t, \dots$. These events consist of outflow, inflow, and pairing. At each event, $m_{\text{out}} = L\Delta t/\tau_{\text{res}}$ particle pairs (selected at random) flow out of the reactor (i.e., they are discarded). A "candidate pile" is created consisting of $2m_{\text{in}}$ particles with the specified inlet composition (where $m_{\text{in}} = m_{\text{out}}$), and $m_{\text{pair}} = L\Delta t/\tau_{\text{pair}}$ pairs randomly selected from the reactor. Then the particles in the candidate pile are paired randomly, and are then added to the reactor. After this event, the reactor again consists of L pairs of particles.

Between reactor events, the particle compositions evolve continuously. With i and j being the indices of a pair of particles, their compositions evolve according to the equations

$$d\phi^{(i)}/dt = \mathbf{S}(\phi^{(i)}) + (\phi^{(j)} - \phi^{(i)})/\tau_{\text{mix}}, \quad (1)$$

$$d\phi^{(j)}/dt = \mathbf{S}(\phi^{(j)}) + (\phi^{(i)} - \phi^{(j)})/\tau_{\text{mix}}, \quad (2)$$

where $\mathbf{S}$ is the chemical reaction term, and τ_{mix} is the mixing time scale.

Notice that the mixing—i.e., the second terms on the right-hand sides of Eqs. 1 and 2—is between pairs of particles, rather than with the mean (as in the PaSR). Hence we refer to this test case as a pairwise mixing stirred reactor (PMSR). Compared to the PaSR, the particles access a greater region of composition space.

In the calculations reported in Section 6, the PMSR parameters are specified as $M = 100$, $\tau_{\text{res}} = 10^{-2}$ (s), $\tau_{\text{pair}} = 10^{-3}$ (s), $\tau_{\text{mix}} = 10^{-3}$ (s), $\Delta t = 6.0 \times 10^{-4}$ (s).

4. OPERATOR SPLITTING SOLUTIONS FOR THE FULL COUPLING EQUATIONS

In order to use the table-look-up method, it is necessary to split Eqs. 1 and 2 so that for a given composition point, the increment of it only depends on the given value of this composition point and the information about mixing.

Operator splitting techniques, also known as the method of fractional steps, were introduced in fifties [18, 19]. The mathematical foundations are summarized in [20]. Operator splitting methods offer a wide variety for splitting a system. Here we investigated several kinds of operator splitting methods: the zero-order splitting method, the first-order splitting method, predictor-corrector methods, and Strang's sequential splitting method. Splitting errors depend on fractional time steps. To investigate the errors, we divide the time step in the PMSR, Δt, into several subtime steps, δt, $\delta t = \Delta t/n_{\text{sub}}$, where n_{sub} is the number of subtime steps.

For the *zero-order splitting method*, Eqs. 1 and 2 are split into a pure mixing system:

$$d\phi^{(i)}/dt = (\phi^{(j)} - \phi^{(i)})/\tau_{\text{mix}}, \quad (3)$$

$$d\phi^{(j)}/dt = -(\phi^{(j)} - \phi^{(i)})/\tau_{\text{mix}}, \quad (4)$$

and a pure chemical reaction system:

$$d\phi^{(i)}/dt = \mathbf{S}(\phi^{(i)}), \quad (5)$$

$$d\phi^{(j)}/dt = \mathbf{S}(\phi^{(j)}). \quad (6)$$

In the first fractional step, the pure mixing system is integrated over a time step δt, to get $\phi_{\text{mix}}^{(i)}$ and $\phi_{\text{mix}}^{(j)}$; then, in the second fractional step, the pure reaction system is integrated (from initial conditions $\phi_{\text{mix}}^{(i)}$ and $\phi_{\text{mix}}^{(j)}$) over a time step δt to get $\phi^{(i)}(t + \delta t)$ and $\phi^{(j)}(t + \delta t)$. The traditional table-look-up method is basically this zero-order splitting method.

For the *first-order splitting method*, the first fractional time step is the same as that in the zero-order splitting method. The values of $\phi_{\text{mix}}^{(i)}$ and $\phi_{\text{mix}}^{(j)}$ are obtained after the first fractional step. In the second fractional step, the system is split as

$$d\phi^{(i)}/dt = \mathbf{S}(\phi^{(i)}) + \mathbf{F}, \quad (7)$$

$$d\phi^{(j)}/dt = \mathbf{S}(\phi^{(j)}) - \mathbf{F}, \quad (8)$$

where $\mathbf{F}$ is the constant mixing vector defined as:

$$\mathbf{F} = (\phi_{\text{mix}}^{(j)} - \phi_{\text{mix}}^{(i)})/\delta t. \quad (9)$$

This system is integrated over a time step δt to get the solutions $\phi^{(i)}(t + \delta t)$ and $\phi^{(j)}(t + \delta t)$.

Two different predictor-corrector methods were investigated. For both methods, the first fractional step is the same as that in the first-order splitting method. In the second fractional step, for the *first predictor-corrector* method, the split systems Eqs. 7 and 8 are integrated over a time step δt to get the predict values: $\phi_p^{(i)}$ and $\phi_p^{(j)}$; then the mixing vector **F** is calculated based on $[\phi^{(i)}(t) + \phi_p^{(i)}]/2$ and $[\phi^{(j)}(t) + \phi_p^{(j)}]/2$; in the corrector step, the split systems are solved over a time step δt to get the final solutions $\phi^{(i)}(t + \delta t)$ and $\phi^{(j)}(t + \delta t)$.

For the *second predictor-corrector* method in the second fractional step, the split systems Eqs. 7, 8 are integrated over half the time step $\delta t/2$ to get the predict values: $\phi_p^{(i)}$ and $\phi_p^{(j)}$; then the mixing vector **F** is calculated based on $\phi_p^{(i)}$ and $\phi_p^{(j)}$. In the corrector step, the split systems are integrated over a full time step δt to get the solutions $\phi^{(i)}(t + \delta t)$ and $\phi^{(j)}(t + \delta t)$.

Strang's sequential splitting method [21] is performed as follows: advance the pure mixing system by half the time step, $\delta t/2$, to get $\phi_{\text{mix}}^{(i,1/2)}$ and $\phi_{\text{mix}}^{(j,1/2)}$; then starting from these conditions, integrate the pure reaction system over a full time step, δt, to get $\phi_{\text{rec}}^{(i)}$ and $\phi_{\text{rec}}^{(j)}$; finally, from these conditions, integrate the pure mixing system by half the time step, $\delta t/2$, to get $\phi^{(i)}(t + \delta t)$ and $\phi^{(j)}(t + \delta t)$. This method can also be thought of as mix-react-mix.

The numerical errors incurred in these different methods have been quantified, and are presented in Section 6.

5. SOLUTIONS OF THE SPLIT SYSTEMS BASED ON MANIFOLD POINTS

5.1. Manifold Points

In order to restrict the points to be tabulated in a relatively small region in the composition space, we represent our solutions by information of manifold points. The manifold method is described in detail in [13]. Manifold methods have been used in the calculations of laminar flames [16, 15] and turbulent flames [7].

For a chemically reacting system, the time scales of reaction processes cover a wide range. For a given point in composition space, because of the existence of fast reaction components, the point moves quickly to a low-dimensional manifold; most of the slow reaction processes take place in the low-dimensional manifold. The low-dimensional manifold is identified by studying the Jacobian matrix of the chemical reaction source term, **S**. This is shown in the following.

Let the composition of a particle be $\phi = \{Y_1, Y_2, \ldots, Y_{n_s}, h\}^T$, where Y_i, $i = 1, 2, \ldots, n_s$, is the mass fraction of species i, n_s is the number of species, and h is the specific enthalpy. Let $n = n_s + 1$ be the dimension of ϕ. For a homogeneous, adiabatic, isobaric system, the evolution of ϕ is determined by the equation:

$$\frac{d\phi}{dt} = \mathbf{S}, \tag{10}$$

where **S** is the source term due to chemical reactions (with enthalpy conservation giving $\mathbf{S}_n = 0$). For a given composition point, ϕ, the Jacobian matrix **J** is

$$\mathbf{J} = \left\{ \frac{\partial \mathbf{S}_i}{\partial \phi_j} \right\}. \tag{11}$$

The Jacobian matrix has n eigenvalues, λ_i, $i = 1, 2, \ldots, n$, and the corresponding n eigenvectors. These eigenvalues identify n timescales of the movement of a particle in composition space. The corresponding eigenvectors define the directions associated with the eigenvalues [13]. A manifold point in the composition space is the point at which the movements in directions corresponding to small timescales vanish.

It is common sense that for a chemical reaction system, in some regions of the composition space, the movement goes very fast, as those near equilibrium; while in other regions of the composition space, reactions progress slowly. If we use a fixed dimension for the manifold in the whole composition space, large errors can be expected in slow reaction regions. So it is preferable to change the dimension of a manifold according to the reaction rate. This can be done by introducing a time

scale τ^*. The time scale τ^* should be smaller than the smallest fluid-mechanical time scale in the problem, here the mixing time scale τ_{mix}.

At every point in the composition space a *fast subspace* and a *slow subspace* are defined based on τ^* and the eigenvalues and eigenvectors of the Jacobian $\mathbf{J}$ at that point. If the eigenvalue λ_i has real part greater than $-1/\tau^*$ (i.e., $\text{Re}(\lambda_i) > -1/\tau^*$), then the corresponding eigenvector is in the slow subspace. Conversely, if $\text{Re}(\lambda_i) \leq -1/\tau^*$, then the corresponding eigenvector is in the fast subspace. We denote by n_m the number of eigenvalues with $\text{Re}(\lambda_i) > -1/\tau^*$: so that n_m is the dimensionality of the slow subspace. The dimensionality of the fast subspace is $n_f = n - n_m$. Put another way, the fast and slow subspaces are the invariant subspaces of $\mathbf{J}$ corresponding to eigenvalues with real part less than, and, respectively, greater than, $-1/\tau^*$.

The eigenvectors can be taken as basis vectors in the two subspaces, but computations are more stable if orthonormal bases are employed. Let the orthonormal basis for the slow subspace be:

$$\mathbf{V}^s = \left[\mathbf{q}_1^s, \mathbf{q}_2^s, \ldots, \mathbf{q}_{n_m}^s \right], \quad (12)$$

and let

$$\mathbf{V}^f = \left[q_1^f, q_2^f, \ldots, \mathbf{q}_{n_f}^f \right], \quad (13)$$

be the orthonormal basis for the fast subspace. $\mathbf{V}^s$ and $\mathbf{V}^f$ can be readily computed by the Schur decomposition method [22]. It is briefly described below.

The Jacobian matrix $\mathbf{J}$ can be decomposed by the Schur decomposition into the following form:

$$\mathbf{Q}^T \mathbf{J} \mathbf{Q} = \mathbf{D} + \mathbf{N}, \quad (14)$$

where, $\mathbf{Q}$ is a $n \times n$ unitary matrix, $\mathbf{D} = \text{diag}(\lambda_1, \lambda_2, \ldots, \lambda_n)$, and $\mathbf{N}$ is a $n \times n$ strictly upper triangular matrix. If $\mathbf{Q}$ is partitioned like:

$$\mathbf{Q} = [\mathbf{q}_1, \mathbf{q}_2, \ldots, \mathbf{q}_n], \quad (15)$$

then $\mathbf{q}_i$ are referred to as Schur vectors [22]. If in the matrix $\mathbf{D}$, the eigenvalues are organized

in the order of descending real parts, then the subspace spanned by the first n_m Schur vectors, $\mathbf{q}_1^s, \mathbf{q}_2^s, \ldots, \mathbf{q}_{n_m}^s$, is the slow invariant subspace. If in the matrix $\mathbf{D}$, the eigenvalues are organized in a different way such that the n_f eigenvalues with the smallest real parts appear first in $\mathbf{D}$, then the corresponding subspace spanned by the first n_f Schur vectors $\mathbf{q}_1^f$, $\mathbf{q}_2^f, \ldots, \mathbf{q}_{n_f}^f$, is the fast invariant subspace [22].

Taking the reaction-rate vector $\mathbf{S}$ as an example, any n-vector can be expressed as the sum of slow and fast components

$$\mathbf{S} = \mathbf{S}^s + \mathbf{S}^f. \quad (16)$$

Here, $\mathbf{S}^s$ and $\mathbf{S}^f$ are in the slow and fast subspaces respectively. Consequently, $\mathbf{S}^f$ can be written

$$\mathbf{S}^f = \mathbf{V}^f \hat{\mathbf{S}}^f, \quad (17)$$

where $\hat{\mathbf{S}}^f$ is an n_f-vector giving the components of $\mathbf{S}^f$ in the $\mathbf{V}^f$-basis. These components are determined as follows. Let the $n \times n$ matrix $\mathbf{V}$ be

$$\mathbf{V} \equiv [\mathbf{V}^s \mathbf{V}^f], \quad (18)$$

and let its inverse be

$$\mathbf{V}^{-1} = \mathbf{W} = \begin{bmatrix} \mathbf{W}^s \\ \mathbf{W}^f \end{bmatrix}, \quad (19)$$

where $\mathbf{W}^s$ is an $n_m \times n$ matrix, and $\mathbf{W}^f$ is an $n_f \times n$ matrix. Then the components $\hat{\mathbf{S}}^f$ are given by

$$\hat{\mathbf{S}}^f = \mathbf{W}^f \mathbf{S}. \quad (20)$$

The manifold is defined as the points in the composition space where the fast reactions are equilibrated. In terms of equations, a point on the manifold satisfies $\mathbf{S}^f = 0$, or equivalently $\hat{\mathbf{S}}^f = 0$, or

$$\mathbf{W}^f \mathbf{S} = 0. \quad (21)$$

To summarize, at every point in the composition space, in terms of the local Jacobian $\mathbf{J}$ and the time scale τ^* we define the slow and fast subspaces and the corresponding matrices $\mathbf{V}^s$, $\mathbf{V}^f$, $\mathbf{W}^s$, and $\mathbf{W}^f$. A point is part of the

manifold if, and only if, Eq. 21 is satisfied at that point.

5.2. The Closest Manifold Point

The composition ϕ of a particle in a PDF or PMSR calculation corresponds to a point in composition space. This is usually close to but not exactly on the manifold with the dimension determined by the given time scale τ^*. As mentioned in Section 2, we want to describe the evolution of $\phi^{(0)}(t)$ in terms of quantities on the manifold (which will be tabulated). Hence we need to find the closest manifold point. The closest manifold point $\phi^{(m)}$ of the given point $\phi^{(0)}$ is a point which satisfies the following conditions:

(a) $\phi^{(m)}$ has the same enthalpy and element compositions as $\phi^{(0)}$.
(b) It is on the manifold.
(c) It is realizable, which means that mass fractions of species are non-negative.
(d) It is as close as possible to $\phi^{(0)}$ while satisfying conditions (a) to (c).

Let $\mathbf{W}^s$ and $\mathbf{W}^f$ be the matrices defined by Eq. 19 and let $\mathbf{W}^e$ be the matrix determining the element mass and enthalpy conservation, then the closest manifold point to $\phi^{(0)}$ is determined as the solution $\phi^{(m)}$ to the following problem.

Minimize the 2-norm of $\phi^{(m)} - \phi^{(0)}$, subject to the conditions:

$$\mathbf{W}^e(\phi^{(m)} - \phi^{(0)}) = 0, \tag{22}$$

$$\mathbf{W}^f \mathbf{S}(\phi^{(m)}) = 0, \tag{23}$$

$$\phi_i \geq 0, \qquad i = 1, 2, \ldots, n_s. \tag{24}$$

These equations are solved by an iterative method. Let $\phi^{(i)}$ be the estimate of $\phi^{(m)}$ after the i-th iteration: the next iteration is

$$\phi^{(m)} \simeq \phi^{(i+1)} \equiv \phi^{(i)} + \delta\phi^{(i)} \equiv \phi^{(i)} + \Delta\phi^{(i)}. \tag{25}$$

With $\mathbf{W}$ evaluated at $\phi^{(i)}$, linearize Eq. 23 around $\phi^{(i)}$, write the equations in terms of $\Delta\phi^{(i)}$, Eqs. 22 and 23 become

$$\mathbf{W}^e \Delta\phi^{(i)} = 0, \tag{26}$$

$$[\mathbf{W}^f \mathbf{J}]\Delta\phi^{(i)} = \mathbf{W}^f\{\mathbf{J}(\phi^{(i)} - \phi^{(0)}) - \mathbf{S}(\phi^{(i)})\}. \tag{27}$$

Equations 26 and 27 are underdetermined. Generally, they are solved by the singular value decomposition method to get a minimum norm solution [22]. If this solution has negative mass fractions (in violation of conditions Eq. 24) then instead we use the quadratic programming method [23, 24] to get the minimum norm solution for Eqs. 26 and 27 under constraints (24).

5.3. Coupling Mixing and Reaction in Manifolds

This section describes how the coupling of mixing and reaction are treated to get the value of $\phi^{(0)}(\delta t)$ for a given particle, $\phi^{(0)}$, based on its closest manifold point, $\phi^{(m)}$.

The system obtained from operator splitting methods can be written in the general form:

$$\frac{d\phi}{dt} = \mathbf{S} + \mathbf{F}. \tag{28}$$

For the zero-order splitting system, and the system from Strang's algorithm, $\mathbf{F}$ is zero; for the first order split system, $\mathbf{F}$ is the mixing vector defined by Eq. 9.

With $\delta\phi \equiv \phi - \phi^{(m)}$, the linearization of Eq. 28 about $\phi^{(m)}$ is

$$\frac{d\delta\phi}{dt} = \mathbf{S}(\phi^{(m)}) + \mathbf{J}\delta\phi + \mathbf{F}. \tag{29}$$

The exact solution of this equation is:

$$\delta\phi(\delta t) = \mathbf{A}\,\delta\phi(0) + \mathbf{B}\mathbf{S}(\phi^{(m)}) + \mathbf{B}\mathbf{F}, \tag{30}$$

where the matrices $\mathbf{A}$ and $\mathbf{B}$ are defined by

$$\mathbf{A} = e^{\mathbf{J}\delta t}, \tag{31}$$

$$\mathbf{B} = \int_0^{\delta t} e^{\mathbf{J}(\delta t - \tau)}\, d\tau. \tag{32}$$

Since chemical reactions take place in a wide range on timescale, some processes quickly, it is preferable to represent the second term in the above equation by an exact solution:

$$\delta\phi^R = \int_0^{\delta t} \mathbf{S} \, dt, \tag{33}$$

integrating from the starting point $\phi^{(m)}$. Thus Eq. 30 is modified to:

$$\delta\phi(\delta t) = \mathbf{A}\,\delta\phi(0) + \delta\phi^R + \mathbf{BF}. \tag{34}$$

Due to the wide range of eigenvalues of the Jacobian matrix, difficulties may arise in the calculation of matrices $\mathbf{A}$ and $\mathbf{B}$. The numerical technique used in this paper is the method proposed in [25]. Here is a brief description of the basic idea of the method. According to [25], if

$$\mathbf{C} = \begin{bmatrix} \mathbf{J} & \mathbf{I} \\ 0 & 0 \end{bmatrix}, \tag{35}$$

where $\mathbf{I}$ is an identity matrix of the same order of the matrix $\mathbf{J}$, then, for $\delta t \geq 0$,

$$e^{\mathbf{C}\delta t} = \begin{bmatrix} \mathbf{A} & \mathbf{B} \\ 0 & \mathbf{I} \end{bmatrix}, \tag{36}$$

where $\mathbf{A}$ and $\mathbf{B}$ are the matrices defined by Eqs. 31 and 32. So if the matrix $e^{\mathbf{C}\delta t}$ is calculated, then $\mathbf{A}$ and $\mathbf{B}$ are known. The Padé approximation method [22] is used to calculate $e^{\mathbf{C}\delta t}$.

The procedure mentioned above can be used to calculate the matrices $\mathbf{A}$ and $\mathbf{B}$ when all the eigenvalues of the Jacobian matrix $\mathbf{J}$ are not large compared with the inverse of the time step, $1/\delta t$. If there exist positive eigenvalues that are large compared to $1/\delta t$, then the system is not stable over the time step. This may correspond to the region near ignition where reaction rates increase rapidly. In this situation, a special treatment is needed to solve the linearized system Eq. 29. The composition space is divided into three subspaces: the divergent slow subspace $\mathscr{D}$, the regular slow subspace $\mathscr{S}$ and the fast subspace $\mathscr{F}$. They are determined by Schur decomposition in the same manner mentioned in the section "Manifold Points." For the divergent subspace $\mathscr{D}$, the corresponding eigenvalues are $Re(\lambda_i) \geq 1/\tau^d$, $i = 1, 2, \ldots, n_d$, where n_d is the dimension of the divergent subspace, $\tau^d = \alpha\delta t$ is a time scale of the divergent subspace, α is a small positive value, we chose it to be 0.1, the corresponding matrix is $\mathbf{V}^d$. For the the slow subspace $\mathscr{S}$, the corresponding eigenvalues, $-1/\tau^* < Re(\lambda_i) < 1/\tau^d$, $i = 1, 2, \ldots, n_{\text{slow}}$, here n_{slow} is the dimension of the slow subspace, the corresponding matrix is $\mathbf{V}^s$. For the fast subspace $\mathscr{F}$, the corresponding eigenvalues, $Re(\lambda_i) \leq -1/\tau^*$, $i = 1, 2, \ldots, n_f$, here n_f is the dimension of the fast subspace, the corresponding matrix is $\mathbf{V}^f$. Let

$$\mathbf{V} = [\mathbf{V}^d \, \mathbf{V}^s \, \mathbf{V}^f]. \tag{37}$$

The inverse of the matrix $\mathbf{V}$ is $\mathbf{W}, \mathbf{W} = \mathbf{V}^{-1}$, which can be written as

$$\mathbf{W} = \begin{bmatrix} \mathbf{W}^d \\ \mathbf{W}^s \\ \mathbf{W}^f \end{bmatrix}. \tag{38}$$

For any vector $\mathbf{x}$,

$$\mathbf{W}\mathbf{x} = \begin{bmatrix} \hat{\mathbf{x}}^d \\ \hat{\mathbf{x}}^s \\ \hat{\mathbf{x}}^f \end{bmatrix}, \tag{39}$$

where $\hat{\mathbf{x}}^d, \hat{\mathbf{x}}^s$, and $\hat{\mathbf{x}}^f$, are the components of $\mathbf{x}$ in the bases of the divergent, slow, and fast subspaces. Thus premultiplying the linearized coupling equation Eq. 29 by $\mathbf{W}$, we get

$$\frac{d}{dt}\begin{bmatrix} \delta\hat{\phi}^d \\ \delta\hat{\phi}^s \\ \delta\hat{\phi}^f \end{bmatrix} = \begin{bmatrix} \hat{\mathbf{S}}^d(\phi^{(m)}) \\ \hat{\mathbf{S}}^s(\phi^{(m)}) \\ \hat{\mathbf{S}}^f(\phi^{(m)}) \end{bmatrix} + \begin{bmatrix} \mathbf{D} & 0 \\ 0 & \mathbf{E} \end{bmatrix}\begin{bmatrix} \delta\hat{\phi}^d \\ \delta\hat{\phi}^s \\ \delta\hat{\phi}^f \end{bmatrix}$$
$$+ \begin{bmatrix} \hat{\mathbf{F}}^d \\ \hat{\mathbf{F}}^s \\ \hat{\mathbf{F}}^f \end{bmatrix}, \tag{40}$$

where

$$\begin{bmatrix} \mathbf{D} & 0 \\ 0 & \mathbf{E} \end{bmatrix} = \mathbf{WJV},$$

$\mathbf{D}$ is a $n_d \times n_d$ matrix, $\mathbf{E}$ is a $(n_{\text{slow}} + n_f) \times (n_{\text{slow}} + n_f)$ matrix.

The equation for the components in the divergent subspace is

$$\frac{d\delta\hat{\phi}^d}{dt} = \hat{\mathbf{S}}^d(\phi^{(m)}) + \mathbf{D}\delta\hat{\phi}^d + \hat{\mathbf{F}}^d. \qquad (41)$$

The Euler explicit scheme is used to get

$$\delta\hat{\phi}^d(\delta t)$$
$$= \delta\hat{\phi}^d(0) + \delta t\left[\hat{\mathbf{S}}^d(\phi^{(m)}) + \mathbf{D}\delta\hat{\phi}^d + \hat{\mathbf{F}}^d\right]. \qquad (42)$$

For the slow and fast components, the solution is

$$\begin{bmatrix} \delta\hat{\phi}^s \\ \delta\hat{\phi}^f \end{bmatrix} = e^{\mathbf{E}\delta t}\begin{bmatrix} \delta\hat{\phi}^s(0) \\ \delta\hat{\phi}^f(0) \end{bmatrix} + \int_0^{\delta t} e^{\mathbf{E}(\delta t - \tau)}\,d\tau$$
$$\times \left\{\begin{bmatrix} \hat{\mathbf{S}}^s(\phi^{(m)}) \\ \hat{\mathbf{S}}^f(\phi^{(m)}) \end{bmatrix} + \begin{bmatrix} \hat{\mathbf{F}}^s \\ \hat{\mathbf{F}}^f \end{bmatrix}\right\}. \qquad (43)$$

Replacing the $\hat{\mathbf{S}}(\phi^{(m)})$ terms in Eqs. 42 and 43 by the exact solution

$$\delta\hat{\phi}^R = W\delta\phi^R, \qquad (44)$$

then the increment of the composition vector in the bases of $\mathbf{V}$ is

$$\begin{bmatrix} \delta\hat{\phi}^d \\ \delta\hat{\phi}^s \\ \delta\hat{\phi}^f \end{bmatrix} = \delta\hat{\phi}^R + \begin{bmatrix} \delta\hat{\phi}^d(0) \\ e^{\mathbf{E}\delta t}\delta\hat{\phi}^s(0) \\ e^{\mathbf{E}\delta t}\delta\hat{\phi}^f(0) \end{bmatrix}$$
$$+ \begin{bmatrix} \delta t\left(\mathbf{D}\delta\hat{\phi}^d + \hat{\mathbf{F}}^d\right) \\ \int_0^{\delta t} e^{\mathbf{E}(\delta t - \tau)}\,d\tau\,\hat{\mathbf{F}}^s \\ \int_0^{\delta t} e^{\mathbf{E}(\delta t - \tau)}\,d\tau\,\hat{\mathbf{F}}^f \end{bmatrix}. \qquad (45)$$

So the increment of the composition vector is

$$\delta\phi(\delta t) = \mathbf{V}\begin{bmatrix} \delta\hat{\phi}^d \\ \delta\hat{\phi}^s \\ \delta\hat{\phi}^f \end{bmatrix}. \qquad (46)$$

In summary, Eq. 46 provides a stable and accurate solution to the coupled mixing and reaction equation linearized about the manifold point $\phi^{(m)}$.

6. RESULTS AND DISCUSSIONS

The chemical kinetic mechanism used in the calculations is shown in Table 1 which was used by S. M. Correa at General Electric Research Center. This is a mechanism for methane/air combustion, with sixteen species and forty-one reactions. In our PMSR calculations, the incoming particles to the PMSR are stoichiometric methane/air at 300 K. The pressure of the PMSR is one atmosphere. The particles in the PMSR are initialized to the equilibrium condition. The mixing time scale is $\tau_{\text{mix}} = 10^{-3}$ s, the pairing time scale is $\tau_{\text{pair}} = 10^{-3}$ s, and the residence time scale is $\tau_{\text{res}} = 10^{-2}$ s. The time scale used to determine the dimension of manifolds is $\tau^* = 10^{-4}$ s. There are 100 particles in the reactor, the time step is $\Delta t = 6 \times 10^{-4}$ s.

From direct integrations of Eqs. 1 and 2, the changes of the average mass fractions of all the particles in the PMSR with time are shown in Figs. 1 and 2. Figure 1 shows changes of the average mass fractions of major stable species. Figure 2 shows changes of the average mass fractions of major radicals. It can be seen that after about 0.6 residence times, the average mass fractions reach a statistically steady state. There is some fuel, CH_4, and oxidizer, O_2 in the reactor, while initially none of these reactants exists since the reactor is initialized to the equilibrium conditon. So the statistically steady-state condition of the reactor is significantly different from the equilibrium condition.

Figure 3 shows $\langle|\phi_{DC} - \phi_{D0}|\rangle$ which is the 2-norm of vector $\phi_{DC} - \phi_{D0}$,

$$|\phi_{DC} - \phi_{D0}| = \left\{\sum_{i=1}^{n}(\phi_{DC,i} - \phi_{D0,i})^2\right\}^{1/2},$$

averaged over the particles in the PMSR as a function of time. Here the subscript, D means direct integrations, C means the original full coupling equations (Eqs. 1 and 2), and 0 means zero-order splitting system. The average value, $\langle|\phi_{DC} - \phi_{D0}|\rangle$ is thus defined by

$$\langle|\phi_{DC} - \phi_{D0}|\rangle = \frac{1}{M}\sum_{i=1}^{M}|\phi_{DC}^{(i)} - \phi_{D0}^{(i)}|,$$

TABLE 1

The Chemical Kinetic Mechanism[a]

No.	Reaction	A_n	n	E_n
1	$H + O_2 = OH + O$	1.59E + 17	−0.927	16874.
2	$O + H_2 = OH + H$	3.87E + 04	2.70	6262.
3	$OH + H_2 = H_2O + H$	2.16E + 08	1.51	3430.
4	$OH + OH = O + H_2O$	2.10E + 08	1.40	−397.
5	$H + H + M = H_2 + M$	6.40E + 17	−1.0	0.
6	$H + OH + M = H_2O + M$	8.40E + 21	−2.00	0.
7	$H + O_2 + M = HO_2 + M$	7.00E + 17	−0.80	0.
8	$HO_2 + H = OH + OH$	1.50E + 14	0.0	1004.
9	$HO_2 + H = H_2 + O_2$	2.50E + 13	0.0	693.
10	$HO_2 + O = O_2 + OH$	2.00E + 13	0.0	0.
11	$HO_2 + OH = H_2O + O_2$	6.02E + 13	0.0	0.
12	$H_2O_2 + M = OH + OH + M$	1.00E + 17	0.0	45411.
13	$CO + OH = CO_2 + H$	1.51E + 07	1.3	−758.
14	$CO + O + M = CO_2 + M$	3.01E + 14	0.0	3011.
15	$HCO + H = H_2 + CO$	7.23E + 13	0.0	0.
16	$HCO + O = OH + CO$	3.00E + 13	0.0	0.
17	$HCO + OH = H_2O + CO$	1.00E + 14	0.0	0.
18	$HCO + O_2 = HO_2 + CO$	4.20E + 12	0.0	0.
19	$HCO + M = H + CO + M$	1.86E + 17	−1.0	16993.
20	$CH_2O + H = HCO + H_2$	1.26E + 08	1.62	2175.
22	$CH_2O + O = HCO + OH$	3.50E + 13	0.0	3513.
23	$CH_2O + OH = HCO + H_2O$	7.23E + 05	2.46	−970.
24	$CH_2O + O_2 = HCO + HO_2$	1.00E + 14	0.0	39914.
25	$CH_2O + CH_3 = HCO + CH_4$	8.91E − 13	7.40	−956.
26	$CH_2O + M = HCO + H + M$	5.00E + 16	0.0	76482.
27	$CH_3 + O = CH_2O + H$	8.43E + 13	0.0	0.
28	$CH_3 + OH = CH_2O + H_2$	8.00E + 12	0.0	0.
29	$CH_3 + O_2 = CH_3O + O$	4.30E + 13	0.0	30808.
30	$CH_3 + O_2 = CH_2O + HO_2$	5.20E + 13	0.0	34895.
31	$CH_3 + HO_2 = CH_3O + OH$	2.28E + 13	0.0	0.
32	$CH_3 + HCO = CH_4 + CO$	3.20E + 11	0.50	0.
33	$CH_4 + H = CH_3 + H_2$	7.80E + 06	2.11	7744.
34	$CH_4 + O = CH_3 + OH$	1.90E + 09	1.44	8676.
35	$CH_4 + O_2 = CH_3 + HO_2$	5.60E + 12	0.0	55999.
36	$CH_4 + OH = CH_3 + H_2O$	1.50E + 06	2.13	2438.
37	$CH_4 + HO_2 = CH_3 + H_2O_2$	4.60E + 12	0.0	17997.
38	$CH_3O + H = CH_2O + H_2$	2.00E + 13	0.0	0.
39	$CH_3O + OH = CH_2O + H_2O$	5.00E + 12	0.0	0.
40	$CH_3O + O_2 = CH_2O + HO_2$	4.28E − 13	7.60	−3528.
41	$CH_3O + M = CH_2O + H + M$	1.00E + 14	0.0	25096.

[a] Rate constants are in the form $k_n = A_n T^n \exp[-E_n/(RT)]$, here R is the universal gas constant. Units are moles, cubic centimeters, seconds, Kelvins and calories/mole.
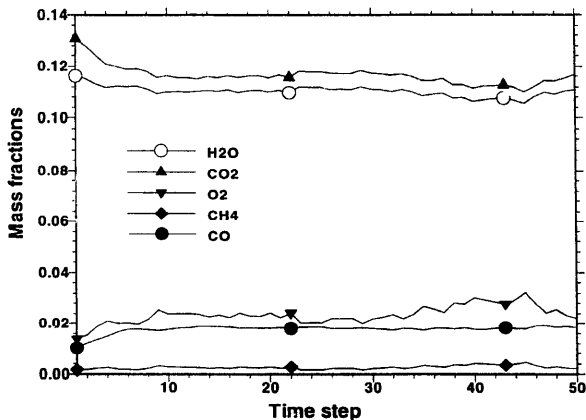
Fig. 1. Average mass fractions of H_2O, CO_2, O_2, CH_4, and CO as functions of time.

where M is the number of particles in the reactor. This is a measure of the error between the solution from the direct integration of the original full coupled equations and the solution from the direct integration of the zero-order splitting system. As shown in the plot, we can see that when the ratio of the subtime step δt to the mixing time scale τ_{mix} decreases, the error uniformly decreases. Figure 4 is a plot of the time average value (from time step 1 to the given time step) of the average error $\langle |\phi_{DC} - \phi_{D0}| \rangle$. After some time, this value becomes a
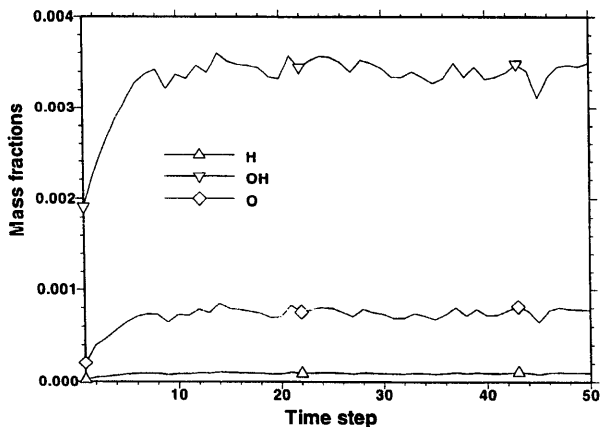
Fig. 2. Average mass fractions of H, OH, and O as functions of time.
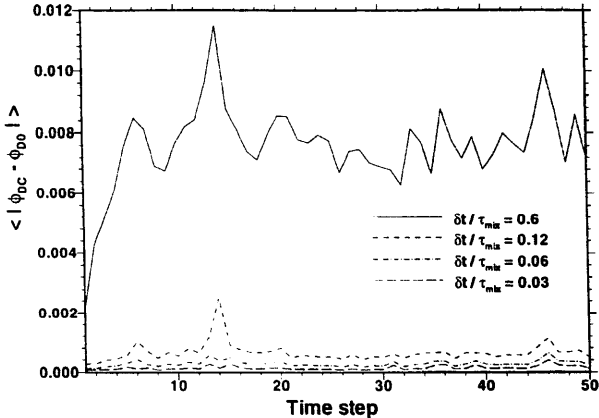
Fig. 3. The average error, $\langle |\phi_{DC} - \phi_{D0}| \rangle$, as a function of time.

constant one. Errors of other methods also behave in the same manner as those of the zero-order splitting system. So we can use the time average value of the errors at time step 50 as a measure of errors of different methods. These are plotted in Figs. 5–7.

In these figures, the first subscript of ϕ indicates D is the direct numerical integration of the equations, M is the solution based on manifold points (i.e., Eq. 46). The remaining subscripts indicate the splitting scheme. C is the full coupled mixing and reaction (no split-
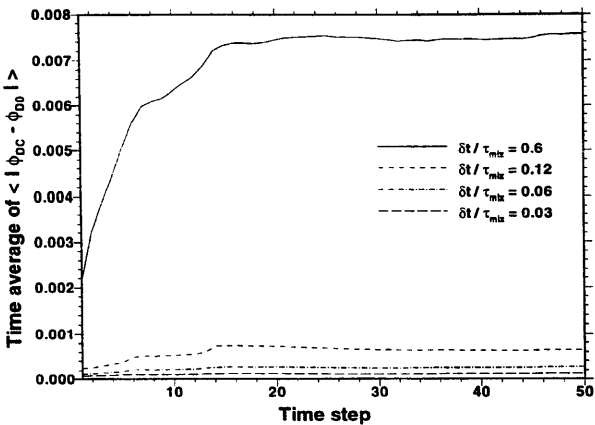
Fig. 4. The time average of the error, $\langle |\phi_{DC} - \phi_{D0}| \rangle$, as a function of time.
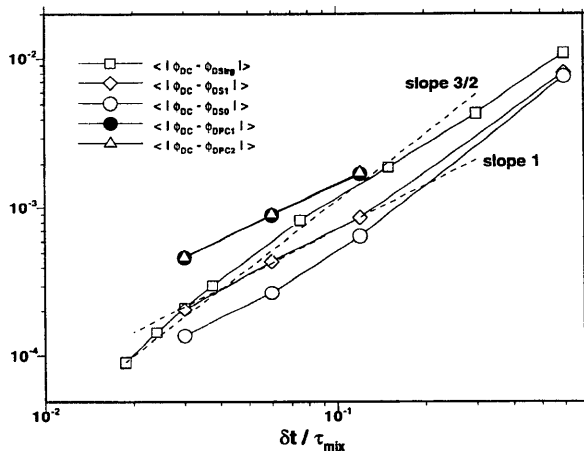
Fig. 5. Variations of splitting errors with the change of the ratio, $\delta t / \tau_{mix}$.

ting), Strg is the system obtained from Strang's sequential splitting method (mix-react-mix), S1 is the system obtained from first-order splitting method, S0 is the system obtained from zero-order splitting method (mix-then-react), PC1 is the system obtained from the first predictor-corrector method, PC2 is the system obtained from the second predictor-corrector method.

There are basically three different types of errors: the splitting errors shown in Fig. 5,
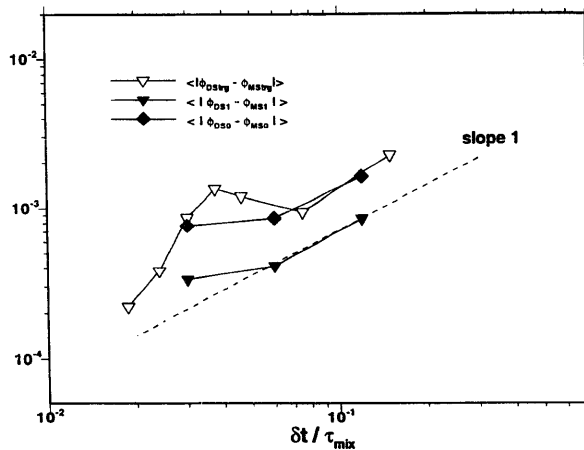
Fig. 6. Variations of chemistry errors with the change of the ratio, $\delta t / \tau_{mix}$.
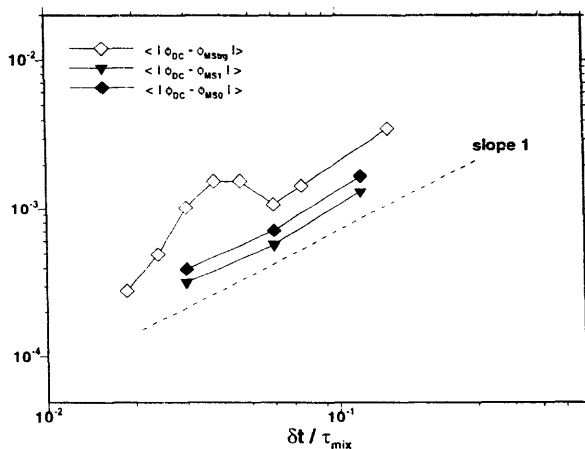
Fig. 7. Variations of over-all errors with the change of the ratio, $\delta t / \tau_{mix}$.

indicated by $\langle |\phi_{DC} - \phi_{Dm}| \rangle$, here m refers to different splitting scheme; the chemistry errors in Fig. 6, showing how well the coupling between chemistry and mixing based on manifold points is doing, they are indicated by $\langle |\phi_{Dm} - \phi_{Mm}| \rangle$; the overall errors in Fig. 7, showing the errors between the solutions from the coupling method based on manifold points and those from direct integration of the original full coupled equations, they are denoted by $\langle |\phi_{DC} - \phi_{Mm}| \rangle$.

It may be seen from Fig. 5 that all of the splitting schemes converge. That is, the errors incurred tend to zero as the time step δt tends to zero. The slope of the curve corresponding to Strang's algorithm is about 1.5, the others are about unity, which means that Strang's method is of order one-and-a-half accurate, the other methods, are first-order accurate. Theoretically, Strang's algorithm and the predictor-corrector methods are of second-order accuracy. The drop in the order of accuracy can be attributed to the fact that the time step used in the calculations, δt, is large compared with the smallest combustion time scales τ_{small} which are represented by negative reciprocals

of the real parts of eigenvalues of the Jacobian matrix $\mathbf{J}$. A typical value of τ_{small} is about 5×10^{-8} (s). The formal order of accuracy is to be expected only when $(\delta t / \tau_{small})$ is small compared to unity, which is not the case here. It is evident from Fig. 5 that the splitting error is smallest for the simple zero-order splitting (S0), i.e., mix-then-react. For the smallest time step shown, these errors are about 0.01% of the major species concentrations.

For selected splitting schemes, Fig. 6 shows the error incurred in using the manifold method (M) compared to direct integration (D). In this case there is no reason to suppose that error tends to zero with δt. For, even in the limit $\delta t \rightarrow 0$, the compositions lie some distance from the manifold, and hence the linearization about manifold points involves some error. (This error does converge to zero as τ^* tends to zero.)

From Fig. 6 we can see that for the zero-order and first-order splitting methods, errors decrease gradually as the ratio of the sub-time step to that of the mixing time scale decreases. For Strang's algorithm, in the region of large $\delta t / \tau_{mix}$, the error decreases with the decreas-

ing of $\delta t/\tau_{\mathrm{mix}}$, as $\delta t/\tau_{\mathrm{mix}}$ decreases further, the error increases, then decreases.

The over-all errors are shown in Fig. 7. These are the errors that we are ultimately interested in as they represent errors of the method compared with direct integrations of the original coupled equations. Errors of the zero-order and first-order splitting methods decrease as $\delta t/\tau_{\mathrm{mix}}$ decreases, the slope of the curves is about unity. The behavior of the over-all error of Strang's algorithm is the same as that of the chemistry error of Strang's algorithm. The chemistry error is the controlling factor for Strang's algorithm.

To give some idea about the change of dimension of the manifold, we plot the manifold dimension n_m versus subtime step for one particle in the PMSR. It is shown in Fig. 8. Plotted together in this figure is the mass fraction of methane for the same particle. The case selected is the first-order splitting method with five sub-time steps. One can see from this figure that most of the time, the dimension of the manifold is 6. The dimension of the conserved subspace is five (four due to element conservation and one due to enthalpy conservation). Thus $n_m = 6$ corresponds to a one-dimensional manifold in the reactive subspace.

Sometimes, the dimension jumps to 14, then decreases to 6 within one time step. The jump of the dimension to high dimension corresponds to the increase in the mass fraction of methane as seen in the figure. In this situation, what happens in the PMSR is that this particle is ejected from the reactor and replaced by an incoming particle which is a mixture of methane and air at stoichiometric condition and room temperature. At these conditions, reactions progress very slowly so the dimension of the manifold is high. As reaction and mixing go on, the composition of the particle moves towards high temperature. So correspondingly, reactions happen faster and the dimension of manifold decreases.

7. CONCLUSIONS

In this paper, different errors of different solution schemes for the original coupled equations of a pair of particles in a pairwise mixing stirred reactor have been investigated. The following conclusions can be drawn:

(1) The pairwise mixing stirred reactor (PMSR) has been formulated as a test case for simplified chemistry schemes. This is a significantly richer and more strenuous test
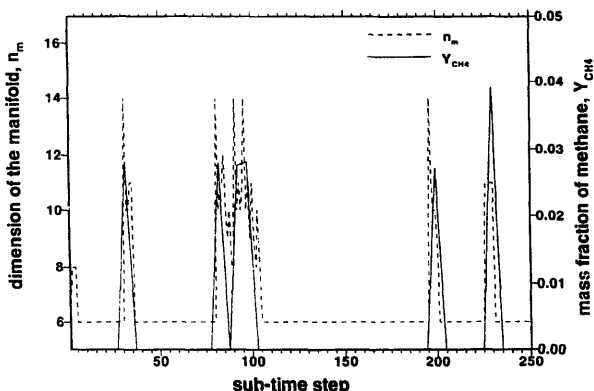

Fig. 8. Changes of the dimension of manifold and methane mass fraction with subtime step.

than the PaSR. (In the statistically-stationary state, the compositions in a PaSR lie on a one-dimensional manifold.)

(2) A variant of the intrinsic low dimensional manifold (ILDM) method has been formulated and used in which the manifold is defined by a time scale τ^*. Rather than having a specified, fixed dimension, the manifold has different dimensions in different regions of the composition space. This results in the manifold method providing an accurate description even in regions where the chemistry is slow.

(3) The "closest manifold point" problem that arises in the implementation of manifold methods has been formulated as a minimization problem, and a reliable iteration algorithm for its solution has been presented and used.

(4) An exact solution (Eq. 30) is given to the coupled reaction-mixing equation, with frozen mixing vector and linearization about the closest manifold point (Eq. 29). A numerically stable solution methodology for this equation has been developed.

(5) Different schemes for splitting reaction and mixing have been investigated. The time step sizes δt of interest are large compared to the smallest time scale of the chemistry τ_{small}. As a consequence, schemes that are formally second-order accurate exhibit lower-order accuracy. All schemes exhibit first-order accuracy except for Strang's algorithm (mix-react-mix) which is of order 3/2.

(6) Over the range of time step size investigated, the simplest zero-order splitting-mix-then-react has the smallest splitting errors, which is as low as 0.01%. This is an important conclusion because it justifies the current practice in table-look-up methodologies.

(7) The combinations of zero-order splitting and the manifold method produce accurate solutions.

REFERENCES

1. Smooke, M. D., *J. Comput. Phy.* 48:72 (1982).
2. Smooke, M. D., *J. Opt. Theory Appl.* 39(4):489 (1983).
3. Smooke, M. D., Miller, J. A., and Kee, R. J., in *Numerical Boundary Value ODEs* (U. M. Ascher and R. D. Russell, Eds.), Birkhauser, Basel, 1985, p. 303.
4. Dixon-Lewis, G., David, T., Gaskell, P. H., Fukutani, S., Jinno, H., Miller, J. A., Kee, R. J., Smooke, M. D., Peters, N., Effelsberg, E., Warnatz, J., and Behrendt, F., *Twentieth Symposium (International) on Combustion*, The Combustion Institute, Pittsburgh, 1984, p. 1893.
5. Pope, S. B., *Prog. Energy Combust. Sci.* 11:119 (1985).
6. Pope, S. B., *Twenty-Third Symposium (International) on Combustion*, The Combustion Institute, Pittsburgh, 1990, p. 591.
7. Norris, A. T., and Pope, S. B., *Combust. Flame* 100:211 (1995).
8. Smooke, M. D., Crump, J., Seshadri, K., and Giovangili, V., *Twenty-Third Symposium (International) on Combustion*, The Combustion Institute, Pittsburgh, 1990, p. 463.
9. Smooke, M. D., Puri, I. K., and Seshadri, K., *Twenty-First Symposium (International) on Combustion*, The Combustion Institute, Pittsburgh, 1986, p. 1783.
10. Peters, N., in *Numerical Simulation of Combustion Phenomena* (R. Glowinski, B. Larrouturou, Temam, Roger, Eds.), Lecture Notes in Physics, Springer-Verlag, Vol. 241, 1985, p. 90.
11. Smooke, M. D., (Ed.), *Reduced Kinetic Mechanisims and Asymptotic Approximations for Methane-Air Flames*, Lecture Notes in Physics, Springer-Verlag, 1991, Vol. 384.
12. Peters, N., and Rogg, B., (Eds.), *Reduced Kinetic Mechanisms for Applications in Combustion Systems*, Lecture Notes in Physics, Springer-Verlag, 1993.
13. Maas, U., and Pope, S. B., *Combust. Flame* 88:239 (1992).
14. Chen, J. Y., Dibble, R. W., and Bilger, R. W., *Twenty-third Symposium (International) on Combustion*, The Combustion Institute, Pittsburgh, 1990, p. 775.
15. Maas, U., and Pope, S. B., *Twenty-Fifth Symposium (International) on Combustion*, The Combustion Institute, Pittsburgh, 1994, p. 1349.
16. Maas, U., and Pope, S. B., *Twenty-Fourth Symposium (International) on Combustion*, The Combustion Institute, Pittsburgh, 1992, p. 103.
17. Correa, S. M., and Braaten, M. E., *Combust. Flame* 94:469 (1993).

18. Douglas, J., *J. Soc. Ind. Appl. Math*. 3:42 (1955).
19. Peaceman, D., and Rachford, H., *J. Soc. Ind. Appl. Math*. 3:28 (1995).
20. Yanenko, N. N., *The Method of Fractional Steps*, Springer-Verlag, Berlin, 1971.
21. Strang, G., *SIAM J. Numer. Anal*. 5(3):506 (1968).
22. Golub, G. H., and Van Loan, C. F., *Matrix Computations*, 2nd ed., Johns Hopkins University Press, Baltimore, 1989.
23. Coleman, T. F., and Y. Li, Cornell Theory Center report CTC92-111, Cornell University, 1992.
24. Land, A. H., *FORTRAN Codes for Mathematical Programming: Linear, Quadratic and Discrete*, John Wiley & Sons, New York, 1972.
25. Van Loan, C. F., *IEEE Trans. Auto. Con*. AC-23(3):395 (1978).